ELSEVIER

Polymer 43 (2002) 4895–4904

polymer

www.elsevier.com/locate/polymer

Study of the interlayer expansion mechanism and thermal–mechanical properties of surface-initiated epoxy nanocomposites

Jir-Shyr Chen, Mark D. Poliks, Christopher K. Ober*, Yuanming Zhang, Ulrich Wiesner, Emmanuel Giannelis

Department of Materials Science and Engineering, Cornell University, Ithaca, NY 14853, USA

Received 15 October 2001; received in revised form 2 May 2002; accepted 8 May 2002

Abstract

The exfoliation mechanism and thermal–mechanical properties of surface-initiated epoxy nanocomposites were studied. Time-resolved high-temperature X-ray diffraction, DSC, and isothermal rheological analyses revealed that the interlayer expansion mechanism might be separated into three stages. These stages relate to the initial interlayer expansion, the steady-state interlayer expansion, and the cessation of interlayer expansion. It was found that differences in the activation energies of interlayer expansion and of curing influence the final nanostructures of the materials. The thermal–mechanical properties of the nanocomposites were studied using dynamic mechanical thermal analysis. Variations in ultimate properties were attributed to the formation of an interphase layer, where the interphase is hypothesized to be the epoxy matrix plasticized by surfactant chains.

Keywords: Epoxy nanocomposite; Exfoliation mechanism; Thermal–mechanical properties

1. Introduction

Nanocomposites based on organically modified layered silicates have proven to be an area of research showing explosive growth in the past decade. This has been due in large part to the sizeable property improvements witnessed in several nanocomposite systems by the addition of only a few weight percent loading of the layered silicates [1–3]. Also, property changes that are normally considered to be inversely related, such as strength and toughness, were found to increase cooperatively in some polymer–clay systems. In general, it is believed that the substantial property improvements result from increased matrix–reinforcement interactions found in nanocomposites as opposed to conventional macroscopic composites.

The clay layers are on the order of 1 nm thick and have extremely high aspect ratios (e.g. 50–1000), thus a few weight percent clay that are properly distributed throughout the polymer system creates significantly more surface area for polymer–filler interactions than do conventional composites [4]. As such, it is also widely accepted that the more separated the clay layers are, the better the overall properties. However, these substantial improvements are not observed in every nanocomposite system, including systems where the silicate layers are completely exfoliated. One polymer system in particular that has improved only marginally through the incorporation of modified silicates is high glass transition temperature (T_g) epoxy thermosets [5–11]. Nominally, high-T_g epoxies can be considered to be epoxy systems with glass transition temperatures greater than room temperature. Such materials are often incorporated into a wide range of applications, including adhesives, coatings, and microelectronic encapsulants [12,13].

In studying nanocomposites based on thermosets, it is important to differentiate between high-T_g materials and subambient-T_g materials. Nanocomposites utilizing rubbery matrix materials tend to exhibit significant property improvements analogous to that previously mentioned, whereas nanocomposites utilizing glassy matrix materials tend to exhibit marginal property improvements, and in some cases degraded properties [6,7]. Lan and Pinnavaia [14] demonstrated that nanocomposites with subambient-T_g's based on a diglycidyl ether of bisphenol-A (DGEBA) epoxy system could exhibit significant property improvements when the proper organically modified silicates were employed. With a clay loading of 15 wt%, the stiffness and strength improved by more than 10-fold. To obtain

* Corresponding author. Tel.: +1-607-255-8417; fax: +1-607-255-6575.
E-mail address: cober@ccmr.cornell.edu (C.K. Ober).

0032-3861/01/$ - see front matter
PII: S0032-3861(02)00318-X

exfoliated nanocomposites, they used the intragallery surfactants for two purposes. The first purpose, which is common amongst almost all layered silicate nanocomposites, was to make the intragallery regions organophillic so as to enable intercalation of the matrix material between the silicate layers. The second function of the surfactants was to catalyze the epoxy polymerization reaction via the onium ions. By having the intragallery polymerization rate comparable to or faster than the extragallery polymerization rate, the clay layers were able to delaminate due to the intragallery crosslinking reactions occurring before the extragallery material crosslinked sufficiently to halt the delamination process. Lan et al. also synthesized high-T_g exfoliated epoxy nanocomposites, again using organically modified layered silicates as catalytic agents [5]. In the glassy state, the nanocomposites exhibited up to a 50% increase in tensile modulus and up to a 4% increase in strength.

An alternate method to obtaining exfoliated epoxy nanocomposites was employed by Messersmith and Giannelis [8]. Instead of using the surfactants solely as a catalytic medium, they also used the hydroxy groups on the surfactants to react with the epoxy groups. By doing so, the matrix polymer was directly bonded to the silicate layers. Compared to the modulus of the pristine epoxy, the modulus of the nanocomposite was 58% higher in the glassy region and 450% higher in the rubbery region. Their results reiterate the general notion that large property improvements typically occur only in rubbery materials.

The objective of the work reported here is to understand the exfoliation mechanism of a high-T_g epoxy nanocomposite and the resulting thermal–mechanical properties. A detailed investigation of the exfoliation mechanism of a surface-initiated epoxy nanocomposite was conducted by using time-resolved high-temperature X-ray diffraction (TT-XRD), dynamic scanning calorimetry (DSC), and isothermal rheometry. These results were coupled with small angle X-ray diffraction studies (SAXS), dynamic mechanical thermal analysis (DMTA), and transmission electron microscopy (TEM) to establish a better understanding of the thermal–mechanical properties of these materials.

2. Experimental

2.1. Materials

3,4-Epoxycyclohexylmethyl-3,4-epoxycyclohexane carboxylate (epoxy monomer), hexahydro-4-methylphthalic anhydride (HHMPA), ethylene glycol (EG), and benzyldimethylamine (BDMA) were used as received from Aldrich Chemicals. The clay used in this study was a montmorillonite modified with a bis-2-hydroxyethyl methyl tallow ammonium cation supplied by Southern Clay under the product name Cloisite 30B (C30B). The as-received C30B was mixed with denatured ethanol to dissolve any excess surfactants that may be present outside of the silicate galleries. The mixture was then centrifuged at 5000 rpm for 10 min prior to decanting the ethanol. The procedure was repeated two more times before drying the clay at 65 °C under vacuum for 4 days. The dried clay was ground with a mortar and pestle and then sifted through a 230 size sieve to collect clay particles smaller than 60 μm in diameter for later use.

2.2. Sample preparation

The epoxy monomer and the curing agent, HHMPA, were mixed in a molar ratio of epoxide groups to HHMPA of 1.00–0.87. The resulting mixture shall be denoted as the *resin*. To the resin was added a specific weight percent of the resin weight of either an initiator (EG), a catalyst (BDMA), or the clay (C30B). The Speedmixer DAC 150FV, an orbital mixer manufactured by Hauschild Engineering, was used to blend the materials at a setting of 2500 rpm for 45 s followed by additional mixing at 3000 rpm for 45 s. A visual inspection revealed the samples to be bubble-free and uniformly mixed. All samples were tested immediately after mixing.

Samples for thermal–mechanical testing were cured in three stages. The samples were first cured isothermally for up to 8 h at temperatures ranging from 70 to 140 °C, followed by 8 h at 180 °C, and finally 12 h at 220 °C under vacuum. The samples were allowed to cool to room temperature at a rate of approximately 1–2 °C/min and were then machined to $20 \times 5 \times 1$ mm^3 pieces for DMTA measurements.

2.3. DSC measurements and extent of reaction calculations

DSC analyses were conducted using a TA Instruments DSC 910. All samples were placed in hermetically sealed aluminum DSC pans and were tested under a nitrogen atmosphere. Dynamic temperature scans were conducted at heating rates of 10 °C/min. For isothermal runs, a temperature ramp of 25 °C/min was used to reach the desired temperature, with a maximum overshoot of approximately +1.5 °C for under 1 min.

The extent of reaction, p, was calculated using two methods [15]. With the first method (Method 1), the samples were measured isothermally. The extent of reaction was calculated by

$$p = \frac{\Delta H(t)}{\Delta H_{\text{Total}}} \tag{1}$$

where $\Delta H(t)$ is the heat generated up to time t and ΔH_{Total} is the total heat generated for the entire reaction. With the second method (Method 2), several samples were cured isothermally for varying lengths of time to create partially cured samples with varying extents of reaction. The samples were then measured in the DSC using dynamic temperature

scans from 30 to 280 °C to measure the residual heats of reaction, ΔH_R. The extent of reaction using Method 2 was calculated by

$$p = \frac{\Delta H_{Total} - \Delta H_R}{\Delta H_{Total}} \quad (2)$$

Due to the low curing temperatures used for some reactions, the heat evolved was too small for accurate detection when using Method 1. Thus, Method 2 was used for all samples requiring quantitative results. Method 1 was used when less quantitative comparisons were needed. It should be noted that errors associated with the extent of reaction calculations using Method 1 were approximately ±5%.

2.4. DMTA and rheology measurements

Samples were measured in both torsional mode and parallel plate mode using a Rheometric Scientific ARES rheometer to determine the materials' thermal–mechanical properties. All measurements were conducted at 1 Hz under a nitrogen atmosphere. Samples for torsional mode experiments were prepared as described above and were tested using a strain amplitude of 0.2% and a 5 °C/min temperature ramp rate. All measurements were conducted while cooling the samples. Isothermal measurements were conducted on uncured as-mixed samples using 25 mm diameter parallel plates and a strain amplitude of 1.0%. The temperature was ramped to the desired isothermal temperature at a rate of 25 °C/min with a maximum overshoot of approximately 1 °C that lasted less than 1 min.

2.5. X-ray diffraction measurements

TT-XRD experiments were conducted using a Bruker-AXS General Area Diffraction Detection System wide-angle X-ray diffractometer with a modified Mettler FP82HT Hotstage attached using custom-made mounts. Sample scan times of 3 min were used for each measurement. Silver behenate, which has a d_{001} diffraction peak corresponding to 58.4 Å, was used to calibrate the setup. Diffraction peaks at low scattering angles ($2\theta < \sim 1.4°$) were distorted, most likely due to air scattering and axial divergence [16]. Thus, the quantitative *d*-spacing range of the setup was from 5 to 58 Å (the calibration limit). However, by comparing diffraction signals obtained from the TT-XRD setup and SAXS results, the effective *d*-spacing detection limits of the TT-XRD setup were determined to be from 5 to 98 Å. SAXS experiments were conducted using a Bruker-AXS Nanostar System. Both the SAXS and TT-XRD setups used Cu irradiation ($\lambda = 1.54$ Å) with X-ray source generators operating at 40 kV and 40 mA.

2.6. Transmission electron microscopy

TEM samples were cut from bulk specimens using a Leica UCT Microtome equipped with a diamond cutting knife. Samples approximately 70 nm thick were analyzed in a JEOL 1200EX TEM with an accelerating voltage of 120 kV.

3. Results and discussions

3.1. Epoxy curing behavior

The curing mechanism for an epoxy–anhydride system with an alcohol initiator is shown in Scheme 1 [17]. Ring-opening of acid anhydrides is initiated by hydroxy groups to form an acid. The acid then ring-opens the epoxy group, thereby yielding another hydroxy moiety to help propagate the polymerization reaction. Amine catalysts like BDMA are often added to the mixture to accelerate the reaction by facilitating the ring-opening of epoxy groups [18]. One purpose of this study was to create exfoliated epoxy nanocomposites and understand the mechanism by which they form by exploiting our knowledge of the established curing reactions. By combining the epoxy–anhydride resin with the organically modified clay (C30B), the anticipated reaction would be that the surfactants located between the clay layers, i.e. the intragallery hydroxy groups, would initiate the polymerization reaction [8].

Several published reports indicate that intragallery onium ions can catalyze the epoxy curing reaction and thus lead to favorable curing conditions for obtaining exfoliated nanocomposites [5,19–22]. Therefore in order to fully understand the interlayer expansion mechanisms of our systems, it was necessary to verify that the crosslinking reactions in the presence of C30B were due to hydroxy initiation and not due to catalytic reactions. To do so, the extent of reaction of a resin containing C30B was compared to the extents of reaction for a neat resin and resins containing either EG or BDMA. As seen in Fig. 1, the curing kinetics of the resin–C30B system more closely resembles the curing kinetics of the resin–EG system than the resin–BDMA system. This is a direct indication that the nanocomposites predominantly cured via initiation by the surfactant hydroxy groups and not by catalytic means. Fig. 1 also shows that the curing rate of the pristine resin is

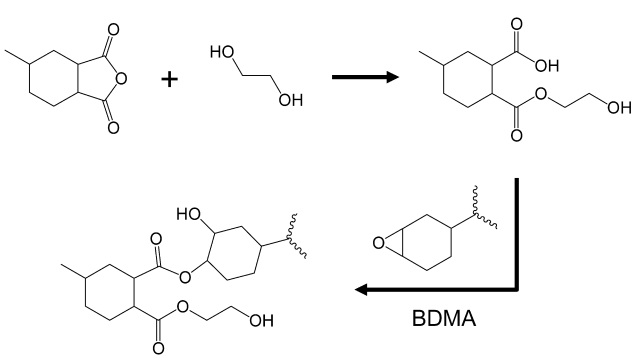

Scheme 1. Generalized curing reaction involving the epoxy monomer, HHMPA, EG, and BDMA.

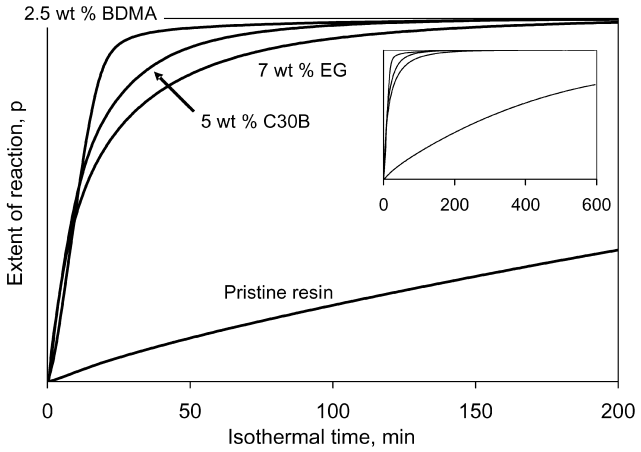

Fig. 1. Extent of reaction of a neat resin and resins containing either C30B, EG, or BDMA. The inset shows the same data but for longer reaction times.

significantly lower than the other mixtures. This highlights an important prerequisite for interlayer expansion, which is that extragallery polymerization rates should be slower than intragallery polymerization rates.

3.2. Layer expansion/exfoliation mechanism

TT-XRD was used to probe the expansion behavior of the silicate layers during curing of the nanocomposites. Fig. 2 shows a plot of the results of a representative data set. To analyze the data, the information was deconvoluted into three components: the d_{001} diffraction intensity, the full-width half-max (FWHM) of the primary diffraction peak, and the rate of d_{001} changes, all with respect to the isothermal cure time. In Fig. 3, the changes in d-spacing are plotted against the isothermal cure time for various clay loadings and cure temperatures. There are several interesting items to note from these results, from which we can separate into three stages of interlayer expansion. The predominant feature of the first stage was the increase then decrease in expansion rate at interlayer spacings less than 45 Å. This trend was most noticeable at lower curing temperatures. The second stage was defined by a linear increase in interlayer spacing with respect to the isothermal

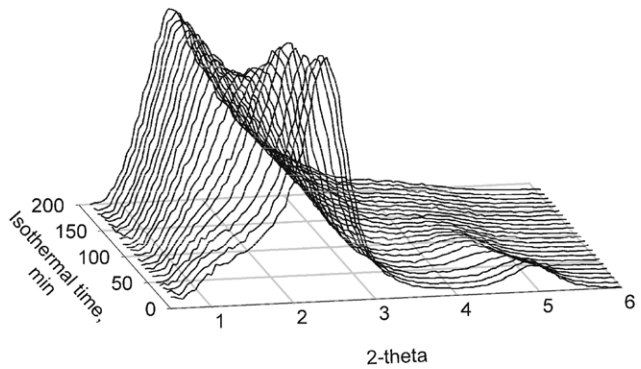

Fig. 2. TT-XRD of a resin containing 15 wt% C30B held isothermally at 70 °C.

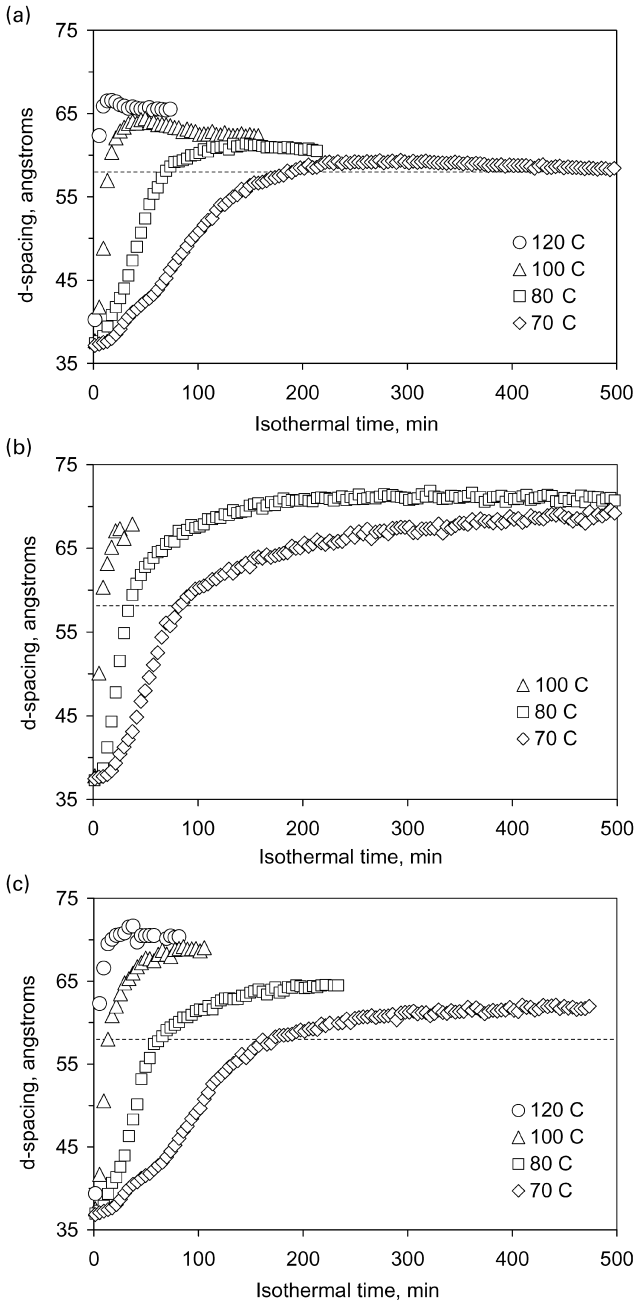

Fig. 3. Changes in d_{001} as a function of the curing time and temperature. From top to bottom, the figures represent clay loadings of 5, 10, and 15 wt%. The dashed lines denote the quantitative detection limit of the TT-XRD setup.

cure time. The third and final stage was characterized by a decrease in the interlayer expansion rate followed by cessation of expansion. In some cases, there was also a subsequent decrease in interlayer spacing of a few angstroms.

3.2.1. Interlayer expansion stage I

The d-spacing of C30B prior to mixing was 18.5 Å. Within the first 5 min after mixing C30B with either the epoxy monomer, HHMPA, or the resin, the d-spacing

increased to 36.5 Å. This initial increase in interlayer spacing is consistent with calculated expansion values where the intragallery surfactant chains assume a nearly-vertical orientation relative to the clay surfaces [5]. Upon heating the different mixtures, the resin–C30B mixtures exhibited an increase in interlayer spacing, whereas the interlayer spacing of the monomer–C30B and HHMPA–C30B mixtures remained constant. This implies that both the epoxy monomer and HHMPA need to be present between the clay layers for an increase in *d*-spacing to occur. It should also be noted that upon heating, resin–C30B mixtures that have sat at room temperature for more than a few hours did not exhibit an increase in *d*-spacing of more than a few angstroms, up to a total interlayer spacing of approximately 41 Å. The most probable explanation for this is that the intercalated resin had polymerized sufficiently to bridge the silicate layers. Due to the high hydroxy concentration attached to the intragallery silicate surfaces, the resin would be expected to begin to react once intercalated, even at ambient temperatures. Also, the diffusion rate of unreacted resin in between the layers is most likely slow enough at these temperatures to prevent significant separation of the layers as the bridges are formed. Therefore upon heating, the bridging units prevented exfoliation of the clay layers and could only stretch and rearrange slightly to accommodate a few angstroms increase in *d*-spacing.

The immediate initiation of polymerization upon intercalation of the resin between the clay layers is also likely to result in the above noted features of the first stage of interlayer expansion. Consider the changes in *d*-spacing, FWHM, and the rate of interlayer expansion in a resin–C30B system as seen in Fig. 4. The 'bump' in the *d*-spacing versus isothermal time plot occurred when the *d*-spacing increased to approximately 40 Å. During the same time interval as the bump, the FWHM remained constant and the rate of expansion decreased to a local minimum. These events may all be explained by a partial and temporary bridging of the silicate layers. Because polymerization is

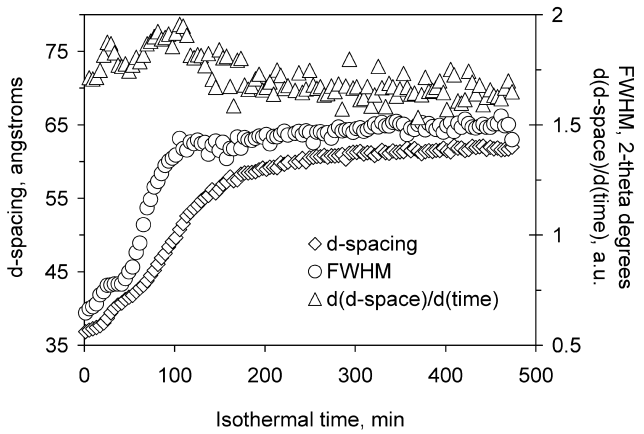

Fig. 4. Changes in d_{001}, FWHM, and the rate of layer expansion plotted as a function of isothermal curing time for a resin with 10 wt% C30B loading tested at 70 °C.

essentially a random event in that the probability of one set of molecules reacting is the same as another, it may be assumed that the formation of bridging units would be distributed randomly throughout the intragallery region. So long as the ambient temperature polymerization is kept to a minimum, the polymerization reaction at higher temperatures would be able to break any of the few bridging chains that may have formed. Therefore, as the curing reaction begins at high temperatures, the clay layers begin to separate and the layer-to-layer registry is decreased, causing the FWHM to increase. As the bridging units are stretched, their resistance to interlayer expansion manifests itself as a decrease in the rate of expansion. Also, assuming the bridging units share a similar length, the degree of layer-to-layer registry should remain relatively constant as the bridging chains are all stretched to their limits, thereby resulting in a nearly constant FWHM. As the bridging units are broken, the interlayer expansion rate and FWHM again increase and the system proceeds to the second interlayer expansion stage. It should be noted that in contrast to many other epoxy systems studied, these networks are cured through ester-based networks. As a result ester interchange can occur at the higher temperatures of curing, leading to breakdown of bridging units.

The bump was not seen in TT-XRD traces collected at higher temperatures because of the time resolution of the experimental setup. Each data point required a 3 min collection time due to the limited intensity of the incident X-ray source. Consequently at higher temperatures, the *stage I* process occurred too quickly to resolve.

3.2.2. Interlayer expansion stage II

The second stage was characterized by a steady and linear increase in *d*-spacing and accounted for most of the total expansion realized. The generally assumed mechanism by which interlayer spacing increases is that as intragallery polymerization proceeds, unreacted material diffuses in between the layers to keep the reaction going and further separate the silicate layers [5,10]. In order to validate the mechanism with our system, isothermal DSC experiments were conducted on freshly mixed resin–C30B mixtures. In Fig. 5, the heat evolved during isothermal DSC scans of a resin with 10 wt% C30B loading are plotted against the isothermal time. A typical isothermal DSC scan for a non-filled thermosetting system exhibits a continuous decrease in heat evolved as the reaction advances, as well as a continuous reduction in the rate of decrease. In the DSC traces of the nanocomposites, there were discontinuities in the heat evolved starting at approximately 12, 30, and 74 min for the 100, 80, and 70 °C scans, respectively. Also, as highlighted with the 70 °C sample in Fig. 5, the starting times and durations of the discontinuities were coincident with their respective linear increases in interlayer spacing. For the rate of heat evolved to remain relatively constant, the polymerized resin within the clay layers, i.e. regions with high concentrations of hydroxy groups, must be rapidly

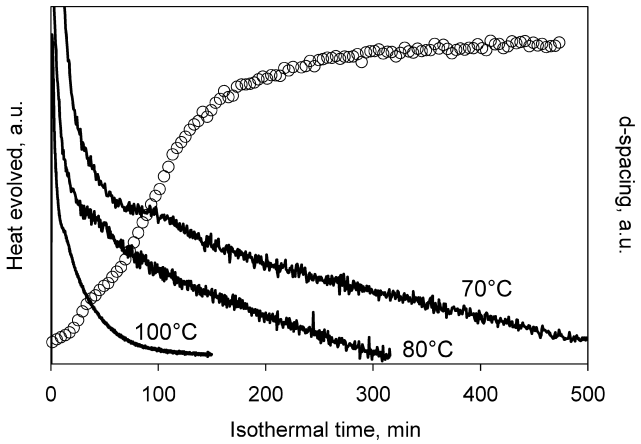

Fig. 5. The solid lines are isothermal DSC scans of a resin with 10 wt% C30B loading. The open circles are the corresponding changes in d_{001} for the 70 °C sample.

replenished by unreacted resin; otherwise, the rate of heat evolved would continue to decrease until polymerization of the nanocomposite was completed. Therefore, the most probable mechanism by which this occurs is via the aforementioned route.

The constant expansion rate in the second expansion stage provided a convenient platform for calculating kinetic properties. As seen in Fig. 3, there were differences in expansion rates depending on the curing temperature and the amount of clay loading. For any given curing temperature the expansion rate increased as the amount of clay loading was decreased, which is consistent with findings by others [23]. The interlayer expansion rates also exhibited an Arrhenius temperature dependence that was used to calculate the activation energy associated with silicate layer separation. In Fig. 6, the natural log of the rate of interlayer expansion is plotted against the reciprocal of the curing temperature for each clay loading. The calculated activation energies for 5, 10, and 15 wt% clay loading are ~75 kJ/mol within experimental error.

Fig. 7 shows the extent of reaction as a function of the

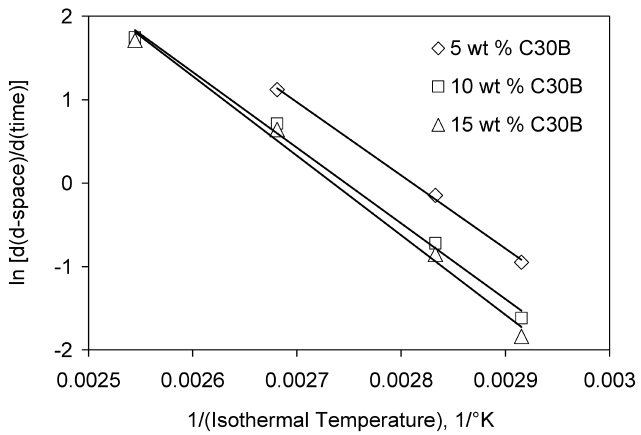

Fig. 6. The natural log of the rate of interlayer expansion plotted against the reciprocal of the curing temperature of various clay loadings. The straight lines are linear fits.

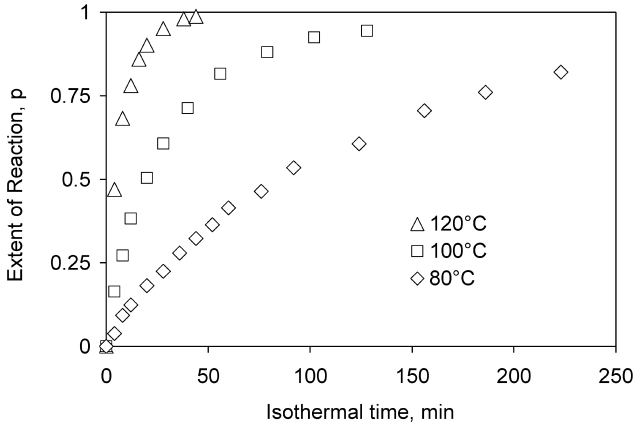

Fig. 7. The extent of reaction plotted against the isothermal cure time for a resin with 10 wt% C30B loading. The figure legend indicates the curing temperature.

isothermal cure time for a resin with 10 wt% C30B loading using three different cure temperatures. The activation energy for the curing process was calculated by using the time to reach any given extent of reaction and the curing temperature. Depending on the extent of reaction used to calculate the activation energy, the activation energy for the curing process ranged from 81 to 85 kJ/mol. As expected, the activation energy associated with interlayer expansion is less than the activation energy for the curing process. If the numbers were reversed, then one would expect little or no expansion to occur. It should be noted that prior attempts at creating exfoliated nanocomposites using resins with a catalyst added resulted in no interlayer expansion. Based on results from similar epoxy systems, the activation energy of curing for the resin–clay–catalyst systems should be less than 70 kJ/mol. These results also imply that interlayer expansion is more favorable at lower curing temperatures, with the ideal situation being where the temperature is high enough for intragallery polymerization to occur and low enough to prevent extragallery polymerization. However, as noted from Fig. 3, lower curing temperatures resulted in lower interlayer spacings. One possible explanation for the observed results is that the rate of diffusion of the resin in between the silicate layers decreases sufficiently to offset any potential benefits associated with lower curing temperatures [5,10]. This issue will be examined further in Section 3.2.3.

3.2.3. Interlayer expansion stage III

The final stage of interlayer expansion began when the rate of expansion diminished and finished when the total interlayer spacing stopped changing. As seen in Fig. 3, the interlayer spacing sometimes decreased slightly before finally coming to rest. In general, the eventual cessation of interlayer expansion is attributed to extragallery polymerization [5]. More specifically, some have ascribed the conclusion of interlayer expansion to gelation of the polymer matrix [24,25]. The amount of clay loading also influences the final interlayer spacing. By assuming that the exfoliation of clay

was due to space filling by the resin, Chin et al. [23] were able to calculate a maximum theoretical interlayer spacing for fully exfoliated nanocomposites. They found that for their epoxy nanocomposite systems, the maximum interlayer spacing decreased from 1700 Å for a 1 wt% loading down to 69 Å for a 20 wt% loading.

Rheological experiments were conducted to gain more insight into the final interlayer expansion stage. In Fig. 8, the storage modulus and loss modulus are plotted against the isothermal cure time at 70 °C of a resin with 10 wt% C30B loading. The storage modulus began to increase rapidly at the start of the second interlayer expansion stage. The rate of interlayer expansion decreased as the storage modulus began to reach its first plateau between 1×10^3 and 1×10^5 dyn/cm^2. This was most likely due to the onset of extragallery gelation. As the curing reaction proceeded, the storage modulus began to increase rapidly again, starting at around 250 min, and approached a second plateau at around 450 min. The second increase in storage modulus was most probably due to vitrification of the polymer matrix. As the material cured, the crosslink density eventually became great enough such that the evolving glass transition temperature surpassed the curing temperature. As this happened, the nanocomposite went from a rubbery polymer system to a glassy polymer system. The storage modulus increased correspondingly. Also, the interlayer spacing stopped expanding during the rubbery-to-glassy transition. This suggests that interlayer expansion stopped when the modulus of the extragallery polymer became equal to or exceeded the modulus of the intragallery polymer. If this is true, then one possible explanation for the decrease in interlayer spacing seen in Fig. 3 is that as the materials cured, the stiffness of the extragallery polymer sufficiently exceeded the stiffness of the intragallery polymer such that the intragallery material became compressed. The subsequent sections detailing the analyses of the thermal–mechanical properties of these materials support this hypothesis.

Fig. 9 shows a TEM micrograph of a resin–C30B nanocomposite containing 2 wt% clay loading that was initially cured at 120 °C. From TEM studies, samples that displayed a d_{001} peak from SAXS experiments only exhibited layered nanostructures. Samples that showed no d_{001} SAXS peaks were observed to contain a mixture of layered nanostructures and exfoliated single silicate sheets. However in general, the nanostructures predominantly consisted of layered sheets instead of exfoliated single sheets, which was expected considering the interlayer expansion mechanism.

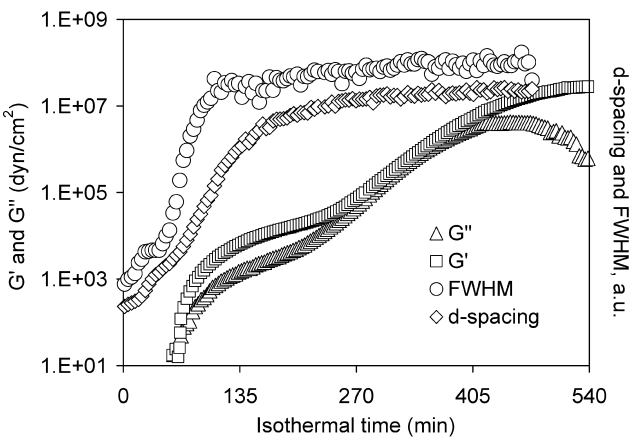

Fig. 8. The storage and loss modulus plotted against the isothermal cure time at 70 °C of a resin with 10 wt% C30B loading. The corresponding changes in d_{001} and FWHM are plotted for comparison.

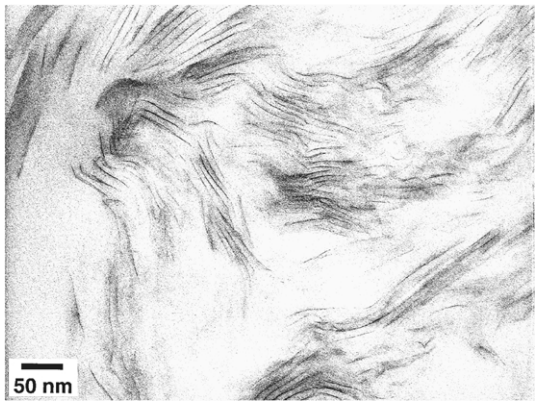

Fig. 9. TEM micrograph showing the nanostructure of a fully cured nanocomposite containing 2 wt% C30B loading initially cured at 120 °C.

Although these results reveal new insights into the interlayer expansion and exfoliation mechanism of epoxy nanocomposites, the fact remains that there are several factors that contribute to the ultimate interlayer spacing of a completely cured material. Consequently, there does not appear to be a simple recipe for creating exfoliated epoxy nanocomposites.

3.3. Thermal–mechanical properties

DMTA conducted in torsional mode was used to determine the nanocomposites' thermal–mechanical properties. Fig. 9 shows the DMTA results of a typical data set. Information obtained from the DMTA experiments are presented in Table 1, as well as the initial cure temperature and the final interlayer spacing for each system (Fig. 10). To determine T_g, the temperature corresponding to the maximum in tan δ was used. The integrated area under the tan δ curve was calculated from $T_g - 70$ to $+70$ °C.

From Table 1, it appears that most of the thermal–mechanical properties of nanocomposites containing 10 and 15 wt% clay loading were highly dependent on the initial cure temperature, whereas samples containing 2 and 5 wt% clay loading were less susceptible to the effects of initial cure temperature.[1] Franco et al. [26] examined the effects of varying the initial cure temperature of a DGEBA epoxy system on T_g, flexural modulus above and below T_g, fracture

[1] The 2 and 5 wt% at 120 °C samples curled upon cooling, indicating that the samples were inhomogeneously mixed and that some of the clay had settled. As a result, the measured properties of those two samples might not accurately reflect the properties of their homogeneously mixed analogs.

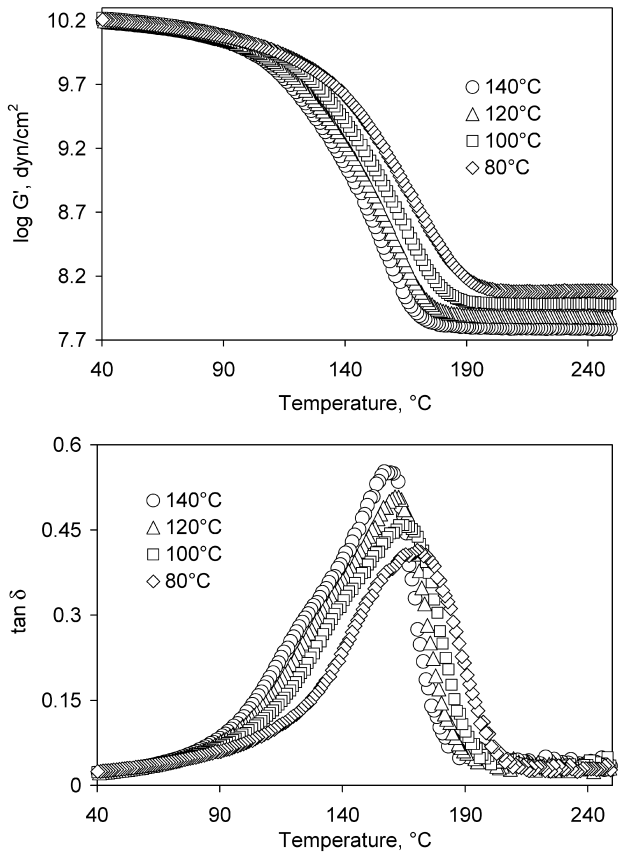

Fig. 10. Top figure shows the log of the storage modulus plotted against the isothermal cure time for resins with 15 wt% C30B loading. The corresponding tan δ plots are shown in bottom figure. The figure legends indicate the initial curing temperature.

toughness, and height of tan δ. They found that varying the initial cure temperature had no significant effects on the final properties of the fully cured resins. Therefore, the property variations in the resin–C30B nanocomposites were most likely due to factors other than varying the initial cure temperature.

The property variations could be due to the formation of an interphase between the silicate layers [27]. An interphase may be defined as the matrix material near the surface of the filler compound, where the properties of the matrix near the surface of the filler differ from the properties in the bulk [28,29]. As mentioned in Section 3.2.1, the surfactant chains were likely to be oriented vertically with respect to the silicate surfaces. Assuming the chains maintained such an orientation as the intragallery resin polymerized, one would expect the chains to plasticize the intragallery polymer. This was alluded to by Shi et al. [30]. Subsequently, assuming the surfactant chains are approximately 37 Å in length [5], the effects of plasticization from the surfactants should persist up to interlayer spacings of at least twice that length, or 74 Å. To get a sense of the effects of plasticization on the ultimate properties of the materials, resins containing varying amounts of EG were examined using DMTA. The results of these experiments are also presented in Table 1.

Figs. 11 and 12 show the changes in T_g and rubbery modulus (storage modulus above T_g), respectively, for nanocomposites with various clay loadings and initial cure temperatures. With the 10 and 15% C30B systems, the T_g and the rubbery modulus decreased as the interlayer spacing increased. With the 5% C30B systems, the T_g and the rubbery modulus were less dependent on the interlayer

Table 1
Thermal–mechanical properties of fully cured resin–C30B nanocomposites and resin–EG mixtures

C30B (wt%)	Init. curing temp. (°C)	d_{001} (nm)[a]	T_g (°C)	tan δ (area)[b]	G' at 40 °C (dyn/cm^2)	G' at T_g + 40 °C (dyn/cm^2)
15	80	6.3	171	25.3	1.61×10^{10}	12.0×10^{7}
15	100	6.9	165	27.6	1.67×10^{10}	9.69×10^{7}
15	120	7.5	161	28.5	1.58×10^{10}	7.76×10^{7}
15	140	7.7	157	30.0	1.54×10^{10}	6.32×10^{7}
10	80	7.5	169	25.2	1.36×10^{10}	9.23×10^{7}
10	100	8.2	166	27.2	1.45×10^{10}	6.69×10^{7}
10	120	9.7	163	28.8	1.48×10^{10}	5.65×10^{7}
10	140	9.8	159	30.5	1.48×10^{10}	4.7×10^{7}
5	80	10.0[c]	157	27.0	1.24×10^{10}	5.74×10^{7}
5	100	10.5[c]	161	27.0	1.22×10^{10}	5.88×10^{7}
5	120	13.0[c]	157	30.4	1.30×10^{10}	3.13×10^{7}
2	80	n.p.[d]	162	25.6	1.21×10^{10}	5.96×10^{7}
2	100	n.p.[d]	163	25.8	1.20×10^{10}	5.80×10^{7}
2	120	n.p.[d]	161	28.8	1.14×10^{10}	3.48×10^{7}
0[e]	120	N/A	227	18.7	1.07×10^{10}	13.0×10^{7}
1[e]	120	N/A	203	19.5	1.03×10^{10}	10.5×10^{7}
2[e]	120	N/A	185	22.7	1.02×10^{10}	7.54×10^{7}
5[e]	120	N/A	148	32.3	1.19×10^{10}	3.19×10^{7}

[a] Determined from SAXS measurements.
[b] Calculated in the range $T_g \pm 70$ °C.
[c] These peaks were not well-defined and are only estimated values based on shoulders detected in the scans.
[d] n.p., no peak detected.
[e] These samples do not contain C30B. The percentages indicates the amount of EG added.

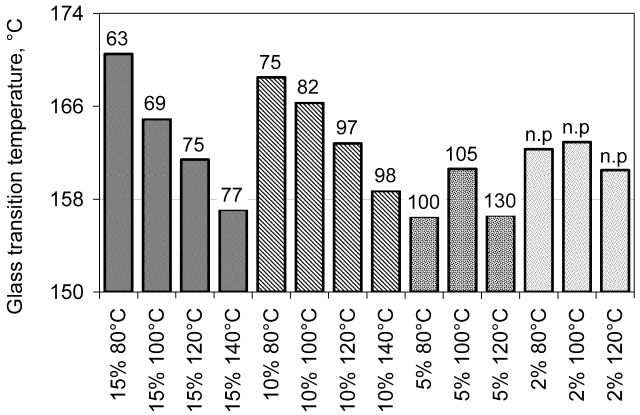

Fig. 11. T_g of fully cured resin–C30B nanocomposites. The number above each column indicates d_{001} for that system. The percentage–temperature labels indicate the weight percent C30B loading and the initial curing temperature.

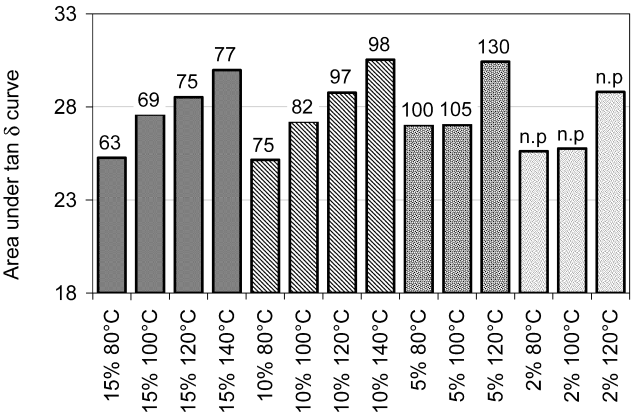

Fig. 13. The integrated area under the tan δ curve. The percentage–temperature labels indicate the weight percent C30B loading and the initial curing temperature.

spacing. Also, among samples with similar interlayer spacings, the samples with lower clay loadings had higher rubbery moduli. These results seem to support the proposed interphase formation. As the interlayer spacing increased, so did the volume percent of interphase material. This led to a decrease in the rubbery modulus and T_g. As the interlayer spacing exceeded 97 Å, the changes in T_g and rubbery modulus became less apparent. This implies that the effects of plasticization from the surfactant chains persist up to approximately 50 Å. The fact that both the T_g and the rubbery modulus varied in a similar fashion with respect to the various clay loadings and initial cure temperatures is not surprising, as it is known that there is a direct relationship between a thermoset's T_g and its rubbery modulus [31–33]. This relationship was also observed in the resin–EG mixtures.

In the glassy region, the effects of the interphase were not readily evident. The moduli below T_g did not exhibit any dependencies on the interlayer spacings, but did vary linearly with the clay loading. In general, variations in crosslink density of a thermoset have little impact on its modulus below T_g [31,33]. Thus, the effects of the stiffness of the silicate layers on the nanocomposite's modulus supercede the effects of the compliancy of the interphase. Compared to the average storage modulus of non-filled resins, the average storage modulus of samples with 15 wt% clay loading was approximately 49% higher. This is comparable to results found by others [6]. A comparison of the moduli of samples above their T_g's cannot be made because the rubbery moduli of the non-filled resins vary greatly depending on the amount of EG added.

The integrated area under the tan δ curve can give an indication of the damping or vibrational energy dissipation capabilities of a material [34]. The calculated areas for the nanocomposites are presented in Fig. 13. As expected, the more compliant materials exhibited larger integrated areas. The effects of interphase formation in nanocomposites are akin to the effects of introducing rubber reinforcement particles into a densely crosslinked epoxy system.

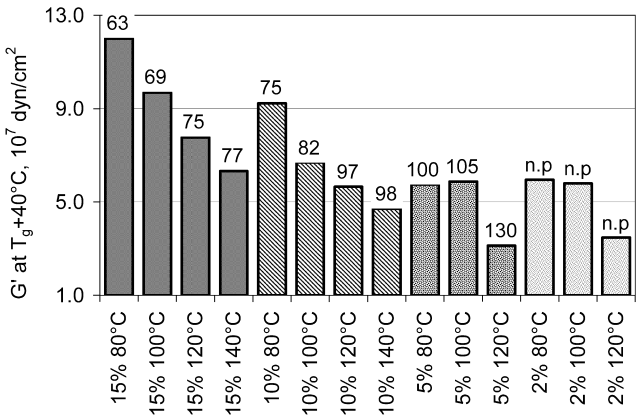

Fig. 12. Storage modulus of fully cured resin–C30B nanocomposites and resin–EG mixtures measured at the materials $T_g + 40$ °C. The percentage–temperature labels indicate the weight percent C30B loading and the initial curing temperature.

4. Conclusions

TT-XRD, DSC, and isothermal rheological analyses were conducted to study the exfoliation mechanism of surface-initiated epoxy nanocomposites. The proposed mechanism consists of three stages. In the first stage, the interlayer expansion induced by intragallery polymerization must overcome any polymer chains that bridge the silicate layers. The interlayer expansion cannot proceed beyond the first stage if the number of bridging units becomes too great. The second stage was characterized by a steady and linear increase in interlayer spacing and accounts for the majority of the total expansion realized. During this stage, the diffusion of unreacted resin in between the silicate layers could be monitored via isothermal DSC experiments. Also, for samples that exhibited large increases in interlayer expansion, it was found that the activation energy associated with interlayer expansion was less than the activation

energy associated with curing. The reverse was true for samples that showed no increase in interlayer spacing. In the third stage, the interlayer expansion slowed then stopped, and in some cases decreased slightly. This was ascribed to the evolving modulus of the extragallery polymer such that the interlayer expansion stopped when the modulus of the extragallery polymer became equal to or exceeded the modulus of the intragallery polymer.

The thermal–mechanical properties of the nanocomposites were studied using DMTA. The drop in T_g and rubbery modulus of samples as the interlayer spacing increased was attributed to the formation of an interphase, where the interphase was hypothesized to be the epoxy plasticized by the surfactant chains. Analyses of property changes as a function of interlayer spacings indicated that the interphase thickness could be as large as 50 Å.

Acknowledgments

Funding from the Semiconductor Research Corporation and IBM Corporation for a fellowship for JSC are gratefully acknowledged. Many thanks are due to M. Weathers and B. Bassett for help with the TT-XRD setup. Thanks are also due to K. Papathomas, G. Kohut, D. Schmidt, and D. Shah for their useful advice and discussions, and to X. Li and M. Li for their help with TEM imaging. Finally, support from the Cornell Center for Materials Research is greatly appreciated.

References

[1] Ellsworth MW, Gin DL. Polym News 1999;24:331–41.
[2] LeBaron PC, Wang Z, Pinnavaia T. J Appl Clay Sci 1999;15:11–29.
[3] Alexandre M, Dubois P. Mater Sci Engng R-Rep 2000;28:1–63.
[4] Giannelis EP, Krishnamoorti R, Manias E, Polymers in confined environments, vol. 138.; 1999. p. 107–47.
[5] Lan T, Kaviratna PD, Pinnavaia T. J Chem Mater 1995;7:2144–50.
[6] Zilg C, Mulhaupt R, Finter J. Macromol Chem Phys 1999;200: 661–70.
[7] Zilg C, Thomann R, Finter J, Mulhaupt R. Macromol Mater Engng 2000;280:41–6.
[8] Messersmith PB, Giannelis EP. Chem Mater 1994;6:1719–25.
[9] Brown JM, Curliss D, Vaia RA. Chem Mater 2000;12:3376–84.
[10] Kornmann X, Lindberg H, Berglund LA. Polymer 2001;42:4493–9.
[11] Zerda AS, Lesser AJ. J Polym Sci, Part B: Polym Phys 2001;39: 1137–46.
[12] May CA. Epoxy resins: chemistry and technology, 2nd ed. New York: Marcel Dekker; 1988.
[13] Seraphim DP, Lasky R, Li C-Y. Principles of electronic packaging. New York: McGraw-Hill; 1989.
[14] Lan T, Pinnavaia T. J Chem Mater 1994;6:2216–9.
[15] Turi EA, 2nd ed. Thermal characterization of polymeric materials, vol. 2.; 1997.
[16] Zevin LS, Kimmel G. Quantitative X-ray diffractometry. New York: Springer; 1995.
[17] Buchwalter SL. Poly Prepr (Am Chem Soc, Div Polym Chem) 1996; 37:186–7.
[18] Matejka L, Lovy J, Pokorny S, Bouchal K, Dusek K. J Polym Sci, Polym Chem 1983;21:2873–85.
[19] Lan T, Kaviratna PD, Pinnavaia T. J Chem Mater 1994;6:573–5.
[20] Lan T, Kaviratna D, Pinnavaia TJ. J Phys Chem Solids 1996;57: 1005–10.
[21] Wang Z, Pinnavaia T. J Chem Mater 1998;10:1820–6.
[22] Wang MS, Pinnavaia T. J Chem Mater 1994;6:468–74.
[23] Chin IJ, Thurn-Albrecht T, Kim HC, Russell TP, Wang J. Polymer 2001;42:5947–52.
[24] Lu JK, Ke YC, Qi ZN, Yi XS. Acta Polym Sin 2000;85–9.
[25] Ke YC, Lu JK, Yi XS, Zhao J, Qi ZN. J Appl Polym Sci 2000;78: 808–15.
[26] Franco M, Corcuera MA, Gavalda J, Valea A, Mondragon I. J Polym Sci, Part B: Polym Phys 1997;35:233–40.
[27] Vaia RA, Giannelis EP. MRS Bull 2001;26:394–401.
[28] Ishida H, editor. Controlled interphases in composite materials. New York: Elsevier; 1990.
[29] Ishida H, Kumar G, editors. Molecular characterization of composite interfaces. Seattle, Washington: Plenum Press; 1983.
[30] Shi HZ, Lan T, Pinnavaia T. J Chem Mater 1996;8:1584.
[31] Murayama T, Bell JP. J Polym Sci, Part A: 2-Polym Phys 1970;8:437.
[32] Bell JP. J Polym Sci, Part A: 2-Polym Phys 1970;8:417.
[33] Nielsen LE. J Macromol Sci-Rev Macromol Chem 1969;C3:69.
[34] Corsaro RD, Sperling LH, editors. Sound and vibration damping with polymers, vol. 424. Washington, DC: American Chemical Society; 1990.